Supporting information for

Hierarchical Assembly of Plasmonic Nanoparticle Heterodimer Arrays with Tunable Sub-5 nm Nanogaps

Jiajing Li[†], *Tian-Song Deng*[‡,§], *Xiaoying Liu*[†], *James A. Dolan*[†,∥,⊥], *Norbert F. Scherer*[‡,§], *Paul F. Nealey*[†,∥,⊥,*]

[†] Pritzker School of Molecular Engineering, University of Chicago, Chicago, IL 60637, USA

[‡] The James Franck Institute, University of Chicago, Chicago, IL 60637, USA

[§] Department of Chemistry, University of Chicago, Chicago, IL 60637, USA

[∥] Material Science Division, Argonne National Laboratory, Lemont, IL 60439, USA

[⊥] Pritzker School of Molecular Engineering, Argonne National Laboratory, Lemont, IL 60439, USA

1. Experimental section

Fabrication of single AuNP arrays. Silicon ⟨100⟩ wafers were purchased from WRS Materials, LLC. Cross-linkable polystyrene (PS) containing 4% glycidyl methacrylate as a crosslinking agent was synthesized as described previously[1]. Hydroxyl-terminated poly(ethylene glycol) methyl ethers (PEG–OH, M_n = 32000 g/mol) was purchased from Polymer Source, Inc. Poly(methyl methacrylate) (PMMA) photoresist (950 kg/mol, 4 wt% in chlorobenzene) was purchased from MicroChem, Inc. AuNPs with citrate ligands were purchased from Ted Pella, Inc. 2-propanol (IPA), 4-methyl-2-pentanone (MIBK), chlorobenzene and 1-methyl-2-pyrrolidinone (NMP) were purchased from Aldrich and used as received.

Substrates were spin-coated from a 0.5 wt% solution of cross-linkable PS in toluene, followed by annealing at 190°C under vacuum for 24 hours to form the crosslinked PS (xPS) mat. Diluted PMMA photoresist (1.5 wt% in chlorobenzene) was then spin-coated on top, and electron beam lithography was performed to create desired dot arrays. After resist development with a mixture of MIBK and IPA (1:3 by volume), the patterned substrates were exposed to oxygen plasma (20 W, 30 s) to remove xPS in the patterned areas. The exposed areas were then functionalized with PEG-OH by spin coating from a 1.5 wt% solution in chlorobenzene and annealing at 200°C for 5 min in a nitrogen atmosphere. The remaining photoresist and excess PEG-OH were removed by sonication in NMP (3 min, 2 cycles) and chlorobenzene (3 min, 1 cycle). For adsorption of AuNPs onto patterned areas, 100 μL AuNP suspension was deposited on the substrate and left still for 40 min in a humid environment. The substrates were then rinsed thoroughly with water and dried with nitrogen.

Synthesis of AuNP-DNA conjugates. NAP-5 columns were purchased from GE Healthcare, Inc. 1,4-dithiothreitol (DTT), sodium chloride (NaCl), sodium dodecyl sulfate (SDS), sodium phosphate monobasic and sodium phosphate dibasic were purchased from Aldrich and used as received. All oligonucleotides were purchased from Integrated DNA Technologies, Inc and are sequenced as follows:

ssDNA1: TAA CAA TAA TCC CTC TTT TTT TTT T-SH

(Cy5-TAA CAA TAA TCC CTC TTT TTT TTT T-SH for Raman scattering measurement)

ssDNA2: GAG GGA TTA TTG TTA TTT TTT TTT T-SH

ssDNA3: SH-T TTT TTT TTT TAC TTT TCA AGT ACT CTG TGA

linker DNA: GAG GGA TTA TTG TTA TCA CAG AGT ACT TGA AAA GTA

AuNP-DNA conjugates were synthesized following a thiol-assisted attachment process as reported previously[2,3]. Briefly, ssDNA2 (or ssDNA3) was treated with 0.1 M DTT solution (pH = 8) for 1 hour and desalted using NAP-5 columns. The purified oligonucleotides were mixed with AuNPs solution (approximately 3000 oligonucleotides/AuNP) and mixed for 1 h on a mixer to form an initial loose loading. The surfactant SDS was then added to the mixture to bring the final concentration of SDS to 0.1%, followed by the addition of 500 mM citrate buffer (pH = 3). After bringing the concentration of citrate buffer to 10 mM, the mixture was placed on a mixer for 2 h for further DNA loading. For a "salt aging" process, 2M NaCl solution was slowly added to the mixture over the next 1 h to bring the final concentration of NaCl to 0.3 M and the solution was allowed to mix for another 2 h. The excess oligonucleotides were removed by three rounds of centrifugation (7000 rpm, 15 min each) and the AuNP-DNA conjugates were resuspended in hybridization buffer (0.3 M NaCl, 0.1% SDS, 0.01 M phosphate buffer, pH = 7).

Fabrication of heterodimer arrays. Arrays of single AuNPs were functionalized with ssDNA1 following a similar procedure as used to synthesize AuNP-DNA conjugates. After treatment with DTT and desalting, purified ssDNA1 was dissolved in a solution of 1 M NaCl, 0.1% SDS and 0.01 M phosphate buffer (pH = 7). The final concentration of oligonucleotides was 2 μM. Substrates were functionalized with single AuNP arrays by soaking in the ssDNA1 solution and being placed on a mixer overnight to complete the DNA loading. After loading is complete, substrates were rinsed by 0.3 M NaCl, 0.1% SDS and distilled water, respectively, and dried with nitrogen. For "15 bps" dimers, the substrates were soaked in solution of AuNP-ssDNA2 conjugates in hybridization buffer (0.3M NaCl, 0.1% SDS, 0.01M phosphate buffer, pH = 7) and placed on a mixer overnight. Following hybridization, the substrates were rinsed with 0.3 M NaCl, 0.1% SDS and distilled water, followed by drying with nitrogen. For "36 bps" dimers, the substrates were first soaked in solution of 2 μM linker DNA in hybridization buffer and mixed for 7 hours to complete hybridization. After rinsing with 0.3 M NaCl, 0.1% SDS and distilled water, the substrates hybridized with AuNP-ssDNA3 conjugates. The assembled structures were imaged by a high-resolution Field-Emission Scanning Electron Microscope (Carl Zeiss Merlin).

Scattering Spectroscopy. Samples were prepared on indium tin oxide (ITO)-coated glass substrates (Structure Probe, Inc) and scattering spectra were measured using a home-built set-up. Prior to scattering measurements, samples were imaged with SEM to determine the direction of the dimer axis. The SEM images were taken at relatively low magnification (15,000×) and short dwell time (6 μs) in a single frame to minimize any potential effect of SEM imaging on the sample. The scattering setup is equipped with a linear polarizer, and the samples were rotated to align the measured dimer axis with the polarization axis of the incident light. A schematic of the set-up for single particle spectroscopy and microscopy is shown in Fig. S1. A broadband white light source

(Fianium, White Lase SC400, 400-2700 nm) was coupled to an inverted optical microscope equipped with an oil immersion objective with numerical aperture NA = 1.4 (Olympus, IX-81; SAPO 100×). The back-scattered images of the sample plane were recorded by a sCMOS array detector (Andor Neo) connected to the eye-piece of the trinocular microscope, and spectra were acquired by an EM-CCD (Andor Newton) connected to an imaging spectrometer (Andor Shamrock 193i) coupled to the side port of the microscope. To minimize the scattering from the coverslip and sample interface, a drop of immersion oil was put on the coverslip, and the inverted sample was placed on top of the immersion oil. Then the coverslip was put on the microscope for measurement. Background correction and normalization were performed for all measurements.

Raman Scattering. Raman spectra were collected on a Horiba LabRAM HR Evolution Raman spectrometer (Horiba, Ltd.) with 633 nm HeNe laser (77.5 μW) and 100× objective. The Raman spectra were recorded in the range of 800–1800 cm^{-1} with 1 s acquisition, 2 accumulations. All data were baseline-corrected by subtracting the background spectra.

Numerical Simulations. FDTD calculations were conducted using FDTD Solutions (Lumerical Solutions, Inc.) software. The simulation set-up is shown in Fig. S2. The environmental refractive index was set as 1.5, corresponding to that of the immersion oil. Gold was simulated using a complex refractive index from Palik et al.[4] and a previously reported model[5] was employed to describe the optical properties of ITO. XPS, PEG brush, and glass were simulated as dielectric materials with real dielectric constants. The spectra were recorded by a frequency-domain field monitor. For simulation of SERS, 633 nm incident light was used instead of broadband white light and the environmental refractive index was set to 1.0 corresponding to that of air.

2. Disentangling the impact of particle size and gap size on distribution of longitudinal plasmon peak positions

A series of simulations were conducted to calculate the longitudinal plasmon resonances of the heterodimers at various gap sizes (from 2 nm to 7 nm) for different size of dimers (from 114 nm to 146 nm). The peak position is approximately linear with gap size and dimer size in the range of calculations:

$$P = a_0 + a_1 G + a_2 R, \quad (1)$$

where P is the peak position in nm, G is the gap size in nm, and R is the size (diameter) of the dimer along the major axis. The variables a_0, a_1 and a_2 are fitting parameters. The adjusted R^2 value of the fitted curve is 0.9522, corresponding to $a_0 = 581.3$, $a_1 = -8.074$, and $a_2 = 0.9081$. Based on equation (1) and the error propagation rules[6], the standard deviation of the peak position may be calculated as

$$\sigma^2(P) = {a_1}^2 \sigma^2(G) + {a_2}^2 \sigma^2(R), \quad (2)$$

where $\sigma(G)$ is the standard deviation of the gap size and $\sigma(R)$ is the standard deviation of the dimer diameter.

Since $R = R_1 + R_2$, where $R_1 = 80$ nm, $R_2 = 50$ nm, and the relative standard deviation of particle size is 8% for both 80 nm and 50 nm AuNPs, as provided by manufacturer, $\sigma^2(R)$ is

$$\sigma^2(R) = \sigma^2(R_1) + \sigma^2(R_2) = (80 \times 0.08)^2 + (50 \times 0.08)^2 = 57 \text{ (nm}^2\text{)}. \quad (3)$$

Since $\sigma^2(P)$ is measured experimentally, $\sigma(G)$ is the only unknown variable in equation (2). We can therefore estimate the standard deviation of gap size $\sigma(G)$ to be 1.0 nm for "15" bps dimers and 0.8 nm for "36 bps" dimers.

Note that the impact of particle shape variation is not included in this calculation, which would contribute another term to (1) and (2), and lead to an even smaller estimate of deviation of gap size.

3. Supplementary figures

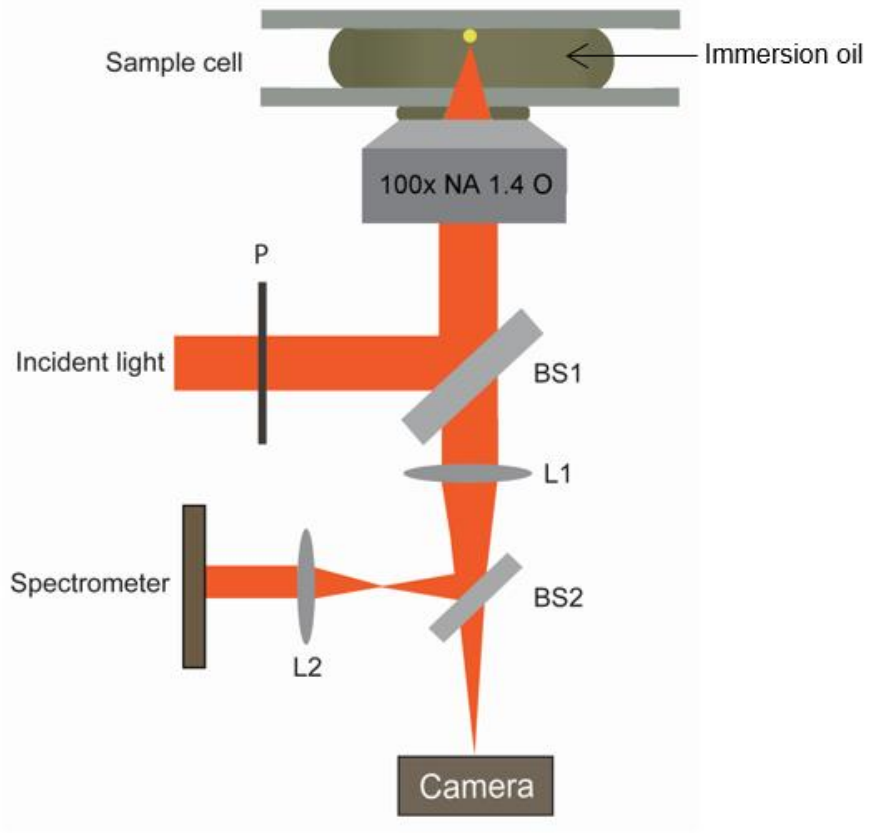

Figure S1. Home built setup for single-particle far-field scattering measurements. P: polarizer, BS: beam splitter, L: lens. A spatially coherent (broadband) white light continuum is coupled to an inverted optical microscope equipped with an oil immersion objective (100×) with numerical aperture, NA ≤ 1.4. The backscattered images and spectra of the sample plane are recorded either by a CCD array detector connected to the eyepiece of the microscope or by a CCD connected to an imaging spectrometer. Note that not all lenses and optical components are shown for simplicity.

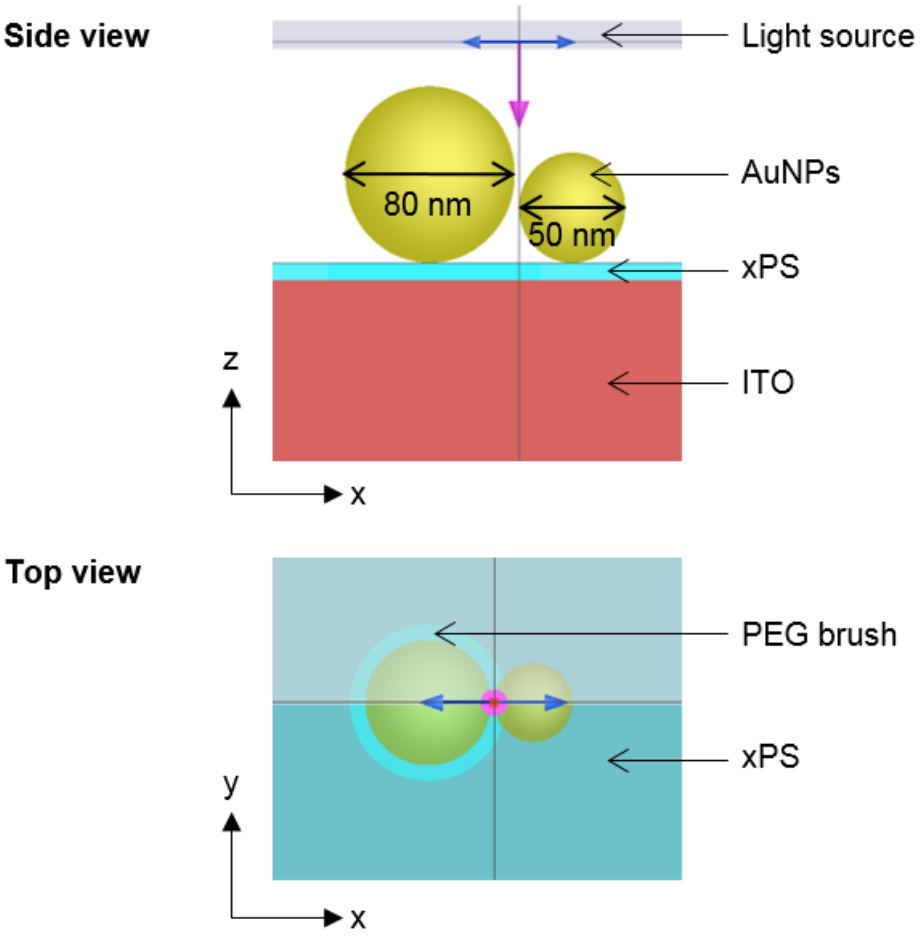

Figure S2. Side view and top view of FDTD simulation. Simulation replicates the experimental configuration. Dielectric functions: Au (Palik[4]), ITO (Konig[5]), xPS (refractive index n=1.59[7]), PEG brush (n=1.46), immersion medium (n=1.5). Dimensions (t=thickness, d=diameter): t_{ITO}=105 nm, t_{xPS}=8 nm, t_{PEG}= 8 nm, d_{PEG}=100 nm. Incident light is polarized along the x axis and spectra are recorded by the frequency-domain field monitor (not shown). Symmetric boundary condition has been chosen for efficiency.

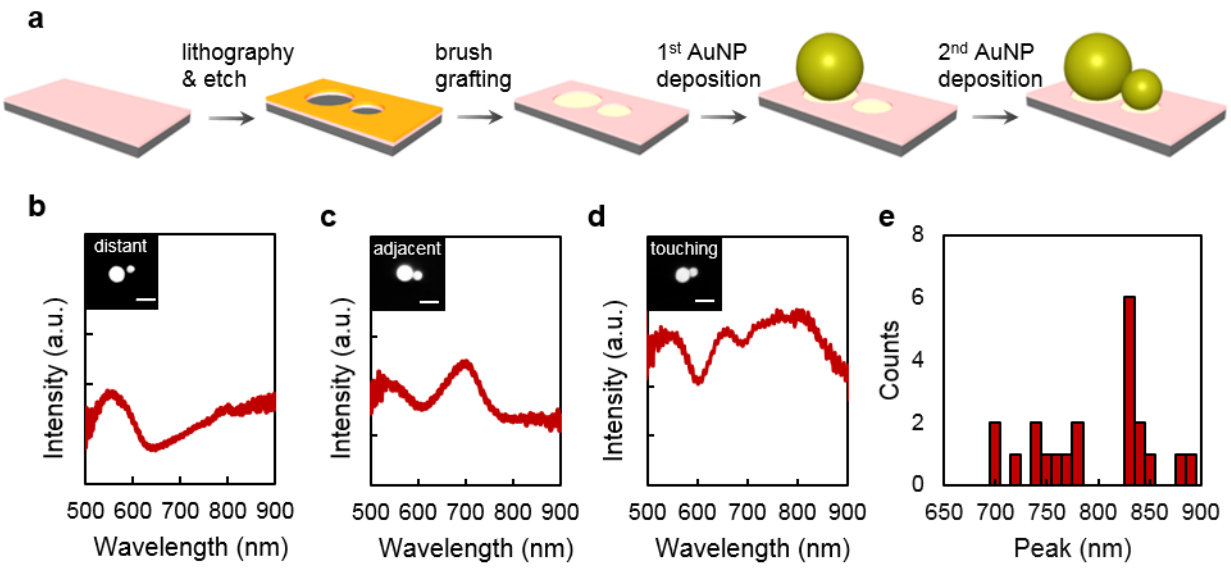

Figure S3. Fabrication of 80-50 nm heterodimers without DNA and the corresponding scattering spectra. (a) Schematic of the process for positioning and patterning AuNPs into heterodimers on chemically patterned substrates without DNA. The assembly solely depends on template-particle interactions and the two AuNPs can be (b) distant from, (c) adjacent to or (d) touching each other, giving rise to one, two or three peaks respectively. (e) A broad distribution of rightmost peak positions indicates that the gaps are much less controlled using this approach compared with hierarchical assembly with DNA included.

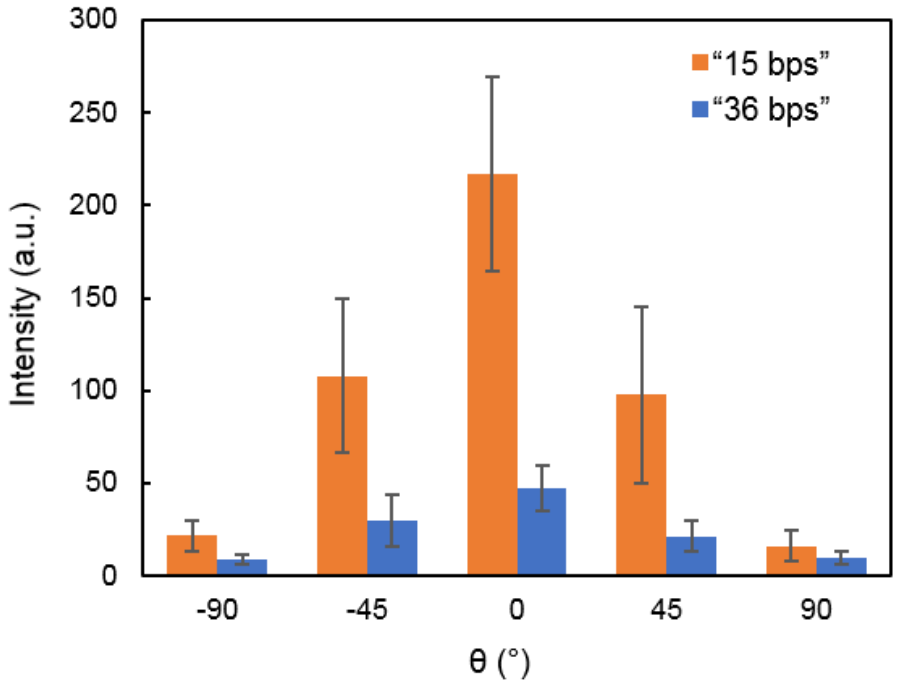

Figure S4. Polarization-dependent SERS intensities at 1589 cm^{-1}. "15 bps" dimers show stronger SERS enhancement than that from "36 bps" dimers due to the associated smaller gap of the heterodimers. Intensities are averaged from five heterodimers for the two types of dimers respectively, and error bars represent one standard deviation.

References

(1) Onses, M. S.; Nealey, P. F. *Small* **2013**, *9* (24), 4168–4174.

(2) Zhang, X.; Servos, M. R.; Liu, J. *J. Am. Chem. Soc.* **2012**, *134* (17), 7266–7269.

(3) Hurst, S. J.; Lytton-Jean, A. K. R. R.; Mirkin, C. A. *Anal. Chem.* **2006**, *78* (24), 8313–8318.

(4) Palik, E. *Handbook of Optical Constants of Solids*; Elsevier, **1997**.

(5) Konig, T. A. F.; Ledin, P. A.; Kerszulis, J.; Mahmoud, M. A.; El-Sayed, M. A.; Reynolds, J. R.; Tsukruk, V. V. *ACS Nano* **2014**, *8* (6), 6182–6192.

(6) Taylor, J. R. *An Introduction to Error Analysis*; University Science Books: Sausalito, CA, **1996**.

(7) Sultanova, N.; Kasarova, S.; Nikolov, I. *Acta Phys. Pol. A* **2009**, *116* (4), 585–587.